Nanoscale

Accepted Manuscript

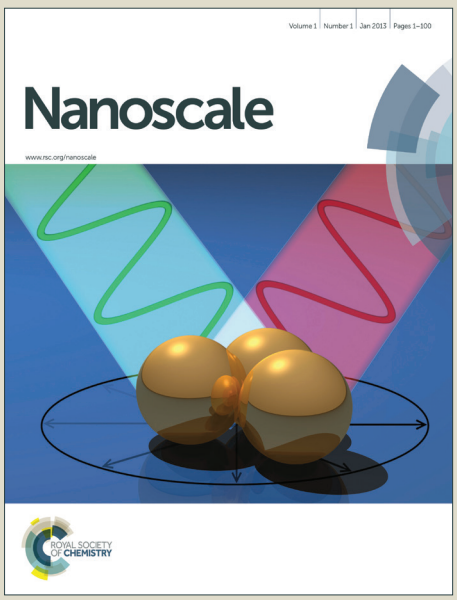

ROYAL SOCIETY OF CHEMISTRY

www.rsc.org/nanoscale

Cite this: DOI: 10.1039/c0xx00000x

www.rsc.org/xxxxxx

ARTICLE TYPE

Definitive proof of graphene hydrogenation by Clemmensen reduction: use of deuterium labeling

Zdeněk Sofer [a,*], Ondřej Jankovský [a], Alena Libánská [a], Petr Šimek [a], Michal Nováček [a], David Sedmidubský [a], Anna Macková [b,c], Romana Mikšová [b,c] and Martin Pumera [d,*]

Received (in XXX, XXX) Xth XXXXXXXXX 20XX, Accepted Xth XXXXXXXXX 20XX
DOI: 10.1039/b000000x

Graphane is one of the most intensively studied derivates of graphene. Here we demonstrate the evaluation of exact degree of graphene hydrogenation using Clemmensen reduction reaction and deuterium labeling. Clemmensen reduction reaction is based on application of zinc in acid environment. It effectively reduces various functional groups (like ketones) present in graphite oxide. However, the mechanism of reduction is still unknown and elusive. Here we bring a major insight into the mechanisms of the Clemmensen reduction via deuterium labeling and topochemical approach applied on graphite oxide. The use of deuterated reactants and exact measurement of deuterium concentration in reduced / hydrogenated graphene by nuclear methods can be used for accurate estimation of C-H bond abundance in graphene. Various topochemical configurations of experiments showed that the reduction of ketonic group proceeds in contact with zinc metal by carbenoid mechanism. Our results showed that the application of nuclear methods of isotope analysis in combination with deuterium labeling represents a very effective tool for investigation of graphene based materials. Our results demonstrate that graphene based materials can be also effectively used for investigation of organic reaction mechanisms, because robust structure of graphene allowed the use of various spectroscopic techniques which could not be applied on small organic molecules.

Introduction

Graphene and its chemical derivatives have been in the forefront of material research in the last decade.[1-4] The great interest is focused on the hydrogenated derivative of graphene – graphane.[5-7] This material belongs to wide-bandgap semiconductor while keeping the 2-dimensional structure of graphene.[6] Several possible applications for this material have been reported manifesting a huge application potential in micro- and optoelectronic, sensor devices and electrochemical energy storage and conversion devices.[8-10]

Recently several procedures for synthesis of hydrogenated graphene have been reported. These methods are based on application of hydrogen plasma,[11, 12] hydrogen treatment at elevated pressure[13] and reaction of solvated electrons with proton source in presence of graphene or some of its derivatives. The latter is typically based on the reaction of water or alcohol with suspension of graphene or graphite in liquid ammonia containing dissolved alkali metal.[14, 15] Another method for graphane synthesis is the reduction of graphite oxide in the presence of acid and electropositive metal. This reaction is known from organic chemistry as Clemmensen reduction.[16]

The Clemmensen reduction is applied in organic synthesis for reduction of ketone groups to methylene groups.[17, 18] The use of zinc in hydrochloric acid environment has been used for the synthesis of chemically reduced graphene.[7, 19] Such a reduction is believed to be accompanied by graphene hydrogenation; however, the proof of hydrogenation is based only on indirect evidence and without exact determination of hydrogenation degree. Even though this reduction method dates to early decades of the last century, the reaction mechanism has not yet been described.[16] The reaction proceeds typically in the presence of zinc (or zinc activated by amalgamation) in hydrochloric acid. For the reaction mechanism two pathways have been generally suggested. In the case of 'carbanionic mechanism' the zinc ion attacks the protonated carbonyl directly in the solution, while in the 'carbenoid mechanism' the reduction takes place on the surface of zinc metal and this reaction has a radical nature.

To investigate the role of Zn in the Clemmensen reduction process, we applied this process on different graphite oxides (GOs) using hydrochloric acid and deuterated hydrochloric acid to investigate the reaction mechanism.[20-23] The reaction of metal with acid leads to hydrogen evolution and a strongly reducing environment is formed. However, the existence and properties of the evolved active hydrogen is

still questioned in the literature. We show here that the reduction takes place only in contact with zinc metal while the role of active hydrogen in the reaction is only marginal. We use the graphite oxide (GO) as a model substrate, since it represents a suitable system for the application of topochemical approach (various arrangement of experiment geometry and rigid substrate suitable for reactions – graphite oxide) and also novel analytical methods can be applied which are not suitable for small molecules. Note that GO is not an "oxide" in the standard chemical sense since it contains a large variety of oxygen containing groups, predominantly epoxy, hydroxyl and ketone groups.[24] The oxygen containing groups of GO have been often used as components for covalent functionalization.[25] However, to the best of our knowledge, there have not yet been any efforts to examine the reaction mechanism using GO. Our observations bring new insight into the mechanism of Clemmensen reaction and demonstrate the synthesis of hydrogenated and deuterated graphene with various degrees of C/H and C/D ratio, respectively.

Experimental

Materials

We used pure graphite microparticles (2–15 μm, 99.9995%, from Alfa Aesar). Sulfuric acid (98%), nitric acid (68%), fuming nitric acid (>98%), potassium chlorate (99%), potassium permanganate (99.5%), sodium nitrate (99.5%), hydrogen peroxide (30%), hydrochloric acid (37%), silver nitrate (99.5%), barium nitrate (99.5%) and N,N-dimethylformamide (DMF) were obtained from Penta, Czech Republic. Deuterium chloride (35% in D_2O, >98%D), deuterium oxide (99.9% D_2O) and Zn powder were obtained from Sigma-Aldrich, Czech Republic.

Synthesis procedure

We prepared four different graphite oxides by four most common methods: Hofmann (HO-GO), Hummers (HU-GO), Brodie (BR-GO) and Staudenmaier (ST-GO).[20-23]

(1) HO-GO. Sulfuric acid (98 %, 87.5 mL) and nitric acid (68 %, 27 mL) were added to a reaction flask (Pyrex beaker with thermometer) containing a magnetic stir bar. The mixture was then cooled by immersion in an ice bath for 30 min. Graphite (5 g) was then added to the mixture with vigorous stirring motion. While keeping the reaction flask in the ice bath, potassium chlorate (55 g) was slowly added to the mixture. Upon the complete dissolution of potassium chlorate, the reaction flask was then loosely capped to allow the escape of the gas evolved and the mixture was continuously stirred for 96 hours at room temperature. The mixture was poured into 3 L of deionized water and decanted. Graphite oxide was then redispersed in HCl solution (5 %, 3 L) to remove sulfate ions and repeatedly centrifuged and redispersed in deionized water until a negative reaction on chloride and sulfate ions was achieved. Graphite oxide slurry was then dried in a vacuum oven (50 °C, 48 hours).

(2) HU-GO. Graphite (5 g) and sodium nitrate (2.5 g) were stirred with sulphuric acid (98 %, 115 mL). The mixture was then cooled to 0 °C. Potassium permanganate (15 g) was then added over a period of two hours. During next four hours, the reaction mixture was allowed to reach room temperature before being heated to 35 °C for 30 min. The reaction mixture was then poured into a flask containing deionized water (250 mL) and heated to 70 °C for 15 minutes. The mixture was then poured into deionized water (1 L). The unreacted potassium permanganate and manganese dioxide were removed by the addition of 3% hydrogen peroxide. The reaction mixture was then allowed to settle and decant. The obtained graphite oxide was then purified by repeated centrifugation and redispersing in deionized water until a negative reaction on sulphate ions was achieved. Graphite oxide slurry was then dried in a vacuum oven (50 °C, 48 hours).

(3) BR-GO. Fuming nitric acid (>98 %, 62.5 mL) was added to a reaction flask containing a magnetic stir bar. The mixture was then subsequently cooled to 0 °C and graphite (5 g) was added. The mixture was stirred to obtain a homogeneous dispersion. While keeping the reaction flask at 0 °C, potassium chlorate (25 g) was slowly added to the mixture. Upon the complete dissolution of potassium chlorate, the reaction flask was loosely capped to allow the escape of the gas evolved and the mixture was stirred for 20 h at 40 °C. Upon completion of the reaction, the mixture was poured into 3 L of deionized water and decanted. Graphite oxide was then redispersed in HCl solution (5 %, 3 L) to remove sulphate ions and repeatedly centrifuged and redispersed in deionized water until a negative reaction on chloride ions was achieved. Graphite oxide slurry was then dried in a vacuum oven (50 °C, 48 hours).

(4) ST-GO. Sulphuric acid (98 %, 87.5 mL) and fuming nitric acid (>98 %, 27 mL) were added to a reaction flask containing a magnetic stir bar. Subsequently, the mixture was cooled to 0 °C and graphite (5 g) was added. The mixture was vigorously stirred to avoid agglomeration and to obtain a homogeneous dispersion. While keeping the reaction flask at 0 °C, potassium chlorate (55 g) was slowly added. Upon the complete dissolution of potassium chlorate, the reaction flask was loosely capped to allow the escape of the gas evolved. Then the mixture was continuously stirred for 96 h at room temperature. The mixture was then poured into deionized water (3 L) and decanted. Graphite oxide was redispersed in HCl solution (5 %, 3 L) to remove sulphate ions and repeatedly centrifuged and redispersed in deionized water until a negative reaction on chloride and sulphate ions was achieved. Graphite oxide slurry was then dried in a vacuum oven (50 °C, 48 hours).

For the reduction 100 mg of GO was dispersed in H_2O and D_2O, respectively, by ultrasonication (400 W, 30 minute). 10 mL of concentrated HCl or DCl and 2.5 g of zinc powder were then added to the dispersion. Reaction mixture was vigorously stirred for 24 hours. In the case of D_2O/DCl the reduction was performed under argon atmosphere. Reduced graphene was separated by suction filtration and washed by diluted hydrochloric acid (1:10 by vol.) and deionized water. Reduced graphene was dried in vacuum oven (60 °C, 48 hours) prior the further use.

Analytical techniques

The morphology was investigated by scanning electron microscopy (SEM) with a FEG electron source (Tescan Lyra dual beam microscope). Elemental composition and mapping were performed using an energy dispersive spectroscopy (EDS) analyzer (X-Max^N) with a 20 mm^2 SDD detector (Oxford Instruments) and AZtecEnergy software. To conduct these measurements, the samples were placed on a carbon conductive tape. SEM and SEM-EDS measurements were carried out using a 10 kV electron beam.

Raman spectroscopy was conducted on an inVia Raman microscope (Renishaw, England) with a CCD detector in backscattering geometry. A DPSS laser (532 nm, 50 mW) with a 100x magnification objective was used for the Raman measurements. The instrument was calibrated with a silicon reference to give a peak position at 520 cm^{-1} and a resolution of less than 1 cm^{-1}.

Combustible elemental analysis (CHNS-O) was performed using a PE 2400 Series II CHNS/O Analyzer (Perkin Elmer, USA). The instrument was used in CHN operating mode (the most robust and interference-free mode) to convert the sample elements to simple gases (CO_2, H_2O and N_2). The PE 2400 analyzer automatically performed combustion, reduction, homogenization of product gases, separation and detection. An MX5 microbalance (Mettler Toledo) was used for precise weighing of the samples (1.5–2.5 mg per single sample analysis). Using this procedure, the accuracy of CHN determination is better than 0.30% abs. Internal calibration was performed using an N-fenyl urea.

Fourier transform infrared spectroscopy (FTIR) measurements were performed on a NICOLET 6700 FTIR spectrometer (Thermo Scientific, USA). A Diamond ATR crystal and DTGS detector were used for all measurements, which were carried out in the range 4000 – 400 cm^{-1}.

High resolution X-ray photoelectron spectroscopy (XPS) was performed using an ESCAProbeP spectrometer (Omicron Nanotechnology Ltd, Germany) with a monochromatic aluminium X-ray radiation source (1486.7 eV). The samples were placed on a conductive carbon tape homogeneously covered with the sample.

For the measurement the samples were compressed in the form of pellets (1/4" diameter, 1 mm thickens). The RBS and ERDA measurements were performed using tandem accelerator Tandetron 4130 MC (¨High Voltage Engineering Europa B.V., Nederland). The RBS measurement was performed with 2 MeV He^+ ions (for C, O and S) and 3.716 MeV He^+ ions (for N). The measurement geometry use 0° entrance angle and 170 ° scattering angle. The ERDA measurement was performed with 2.5 MeV He^+ ions (75° entrance angle and 30° scattering angle). Backscattered ions were detected using ULTRA ORTEC detector placed below entrance beam (Cornell geometry). Canberra PD-25-12-100 AM detector placed in plane with entrance beam (IBM geometry, 12 μm Mylar foil for elimination of He^+ and heavier ions) was used for the detection of forward scattered ions. Theobtained spectra were evaluated using SIMNRA 6.06 and GISA 3.99 software.[26, 27]

Results and discussion

The reduction was performed by zinc dust using aqueous suspension of GO in 1 M hydrochloric acid.[4-7] For the synthesis of deuterium labeled graphenes 1 M deuterium chloride in D_2O was used. The whole experimental procedure is described in detail in the Experimental section. The samples reduced with zinc suspension in acid are named as HO/H/Zn, HO/D/Zn, HU/H/Zn, HU/D/Zn, ST/H/Zn and BR/H/Zn. The first two letters indicate the method of graphite oxide synthesis (HO- Hofmann, HU – Hummers, ST – Staudenmaier, BR – Brodie), while the second part of notation indicates whether the reduction was performed in H_2O/HCl (marked as H) or in D_2O/DCl (marked as D).

We also carried out the reduction of selected graphite oxide (HO-GO) in two different experimental configurations – in the direct contact with zinc and only in the contact with the formed "nascent" hydrogen. The advantage of GO as a substrate is that we can employ "topochemical" reactions. Indeed, performing the chemical reaction on rigid substrate formed by graphite oxide which is brought into contact with zinc as a reducing agent makes it possible to explore various geometries of experimental configuration. Moreover the rigid substrate is suitable for further characterization by analytical methods which could not be applied on small molecules because these freely migrate in the solution and thus one cannot pinpoint whether "nascent" hydrogen plays an active role or the presence of Zn surface is crucial. The process of reduction is illustrated in **Scheme 1**.

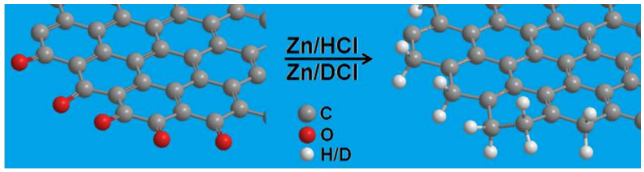

Scheme 1 The process of graphite oxide hydrogenation via Clemmensen reduction reaction.

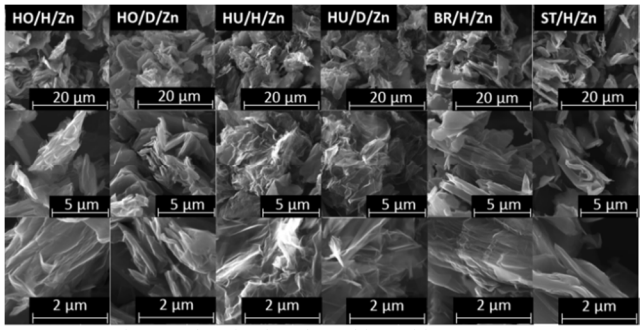

Fig. 1 SEM micrographs of reduced graphite oxides.

The total concentrations of C, H, N and S were obtained by the elemental combustion analysis (**Table 1**). Based on these results we can calculate the minimal concentration of C-H bonds by a simple subtraction of hydrogen and oxygen concentration in atomic percent. In the oxygen functional groups the possible H/O ratio is 1 for hydroxyl groups, 0.5 for carboxylic acids and 0 for ketonic and epoxide groups. The highest difference between C and H and therefore the highest concentration of C-H bonds, 13.68 at.%, was observed for HO/H/Zn, while the lowest concentration of C-H groups was found in ST/H/Zn. A slightly lower concentration of hydrogen measured for deuterated samples originates from the different atomic mass of hydrogen and deuterium resulting in lower concentration of hydrogen observed by elemental combustion analysis. This is in good agreement with the mechanism based on Clemmensen reduction where ketonic groups are reduced / hydrogenated and C-H bonds are formed. However, not only ketonic groups are reduced in graphite oxide, because the GO surface typically contains an appreciable amount of hydroxide and epoxide groups. Particularly the epoxide groups are quite reactive and their reduction led to epoxide ring opening and a simultaneous formation of C-H and C-OH groups on the reduced graphene surface.

Table 1 The composition of graphite oxides exposed to Clemmensen reduction under different conditions (HCl/DCl) by elemental combustion analysis in at.%.

Sample	N	C	H	O	O-H
HO/H/Zn	0	37.86	37.91	24.23	13.68
HO/D/Zn	0.06	39.45	34.15	26.33	7.82
HU/H/Zn	0.12	80.43	11.48	7.97	3.51
HU/D/Zn	0.03	80.65	10.7	8.62	2.08
BR/H/Zn	0.29	48.8	29.7	21.21	8.49
ST/H/Zn	0.19	72.95	13.68	13.17	0.51

The sample morphology was investigated by scanning electron microscopy (SEM). Images taken at different magnification are shown in **Fig. 1**. The morphology of the prepared materials is typical for reduced and exfoliated graphite oxide. As expected, no significant differences were observed between the individual samples.

The presence of C-H bonds was also proved by FT-IR spectroscopy (**Fig. 2**). The FT-IR spectra of starting graphite oxides are shown on **Fig. S1**. The weak effects located at 2900 cm^{-1} and 2950 cm^{-1} are indicative of C-H and C-H_2 groups in the reduced/hydrogenated GO. The spectra acquired for HO-GO and HU-GO reduced in normal or deuterated hydrochloric acid exhibit an almost identical shape suggesting a similar reaction product. Also C=C bond from graphene skeleton represented by a peak at 1540 cm^{-1} and a broad band around 1200 cm^{-1} from remaining hydroxyl groups (C-O vibration band) were detected.

The quality of material from the point of view of defects and the presence of sp^3 bonded carbon were investigated using Raman spectroscopy (**Fig. 3**). The most significant is the presence of D and G bands located at 1360 cm^{-1} and 1560 cm^{-1}, respectively.[28] The intensity of D band is correlated with the presence of defects and carbon in sp^3 hybridization. The G band is associated with sp^2 hybridized carbon in the graphene planar sheet. D/G ratios were calculated from Raman spectra to compare the defects density (**Table 2**). The clear correlation between the degree of oxidation of the starting graphite oxide and D/G ratios was observed. The starting graphite oxide with highest degree of oxidation (HU-GO) also exhibits the highest D/G ratio. Slight differences in higher D/G ratio for samples hydrogenated with hydrogen can be related to the weak isotopic effect where generally heavier deuterium containing molecules have lower reaction rate compared to hydrogen. However, due to very low differences no clear evidence of hydrogen/deuterium kinetic effect was found. The average crystallite size L_a was also calculated from D/G ratios using the equation:[29]

$$L_a = 2.4 \times 10^{-10} \times \lambda_{laser}^{4} \times I_G/I_D \qquad \text{(Eq. 1)}$$

where I_G and I_D denote the respective intensities of the G and D peaks and λ_{laser} is the wavelength of the laser used in nm (**Table 2**).

Table 2. D/G Ratios and corresponding crystallite sizes.

Sample	D/G	Cryst.Size (nm)
HO/H/Zn	1.4	13.7
HO/D/Zn	1.37	14
HU/H/Zn	1.56	12.3
HU/D/Zn	1.5	12.8
BR/H/Zn	1.23	15.6
ST/H/Zn	1.05	18.3

The most suitable method to verify the presence of C-H bonds is the direct measurement of deuterium concentration in the samples synthesized by reduction of graphite oxide in deuterated hydrochloric acid. This experiment was performed using a combined nuclear method of Rutherford back scattering (RBS) and elastic recoil detection analysis (ERDA) (**Fig. 4**). The combination of these two techniques allowed us not only to detect basic elemental composition of light elements (C, H, N) but also to distinguish and quantify the concentration of hydrogen and deuterium within the samples (**Table 3**).

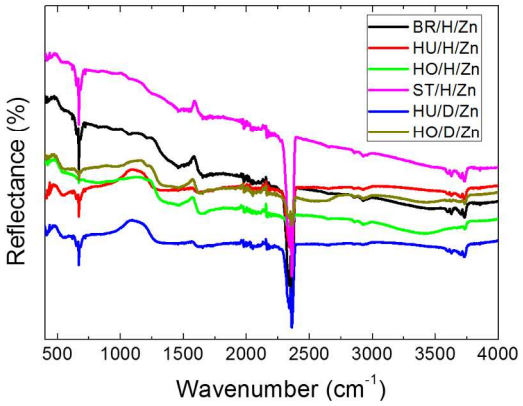

Fig. 2 FT-IR spectra of graphite oxides exposed to Clemmensen reduction under different conditions (HCl/DCl).

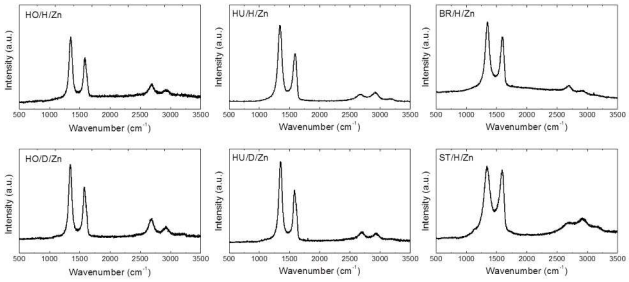

Fig. 3 Raman spectra of reduced graphite oxides.

Table 3 The composition of graphite oxides exposed to Clemmensen reduction under different conditions (HCl/DCl) by Rutherford back scattering and elastic recoil detection analysis in at. %.

Sample	C	O	H	D
HO/H/Zn	64.5	16.1	19.4	0.0
HO/D/Zn	67.8	17.1	3.9	10.8
HU/H/Zn	83.0	7.1	9.9	0.0
HU/D/Zn	80.0	8.9	6.9	4.2
BR/H/Zn	66.3	16.5	17.2	0.0
ST/H/Zn	76.9	13.6	9.5	0.0

The concentration of deuterium was higher in HO/D/Zn (10.8 at.%) compared to HU/D/Zn (4.2 at.%). This is in good agreement with elemental combustion analysis where the highest concentration of C-H bonds was supposed for samples prepared from HO-GO. The higher concentration of C-D bonds in HO/D/Zn can be explained in terms of radical opening of the epoxide ring which led to simultaneous formation of C-D and C-OD bonds. In order to prove that deuterium is present only in the form of C-D bonds and as a part of oxygen functional groups (C-OD), the samples were repeatedly washed with normal water and hydrochloric acid after the reaction. The gradient of hydrogen / deuterium concentration led to an exchange of acidic deuterium (present in -C-OD and -COOD groups) with hydrogen and only C-D bond remained unaffected. HO-GO contained high concentration of reactive oxygen functional groups which undergo reduction/hydrogenation with zinc in acidic environment. This led us to a conclusion that the presence of epoxide and ketone groups is the most important factor for the hydrogenation.

To get a deeper insight into the chemistry of reduced /

hydrogenated graphene we applied high resolution X-ray photoelectron spectroscopy (XPS). A wide range scan was used to obtain the concentration of carbon, oxygen and C/O ratio which indicates the degree of reduction. The dominant peaks are C 1*s* at 284.5 eV and O 1*s* at 532.5 eV (**Fig 5**). The XPS survey spectra of the starting graphite oxides and the corresponding high resolution XPS spectra are shown in SI (**Fig SI3**). The composition of the starting graphite oxides obtained by XPS is shown in Table SI3. The minor F 1*s* peak (at 689 eV) originated from vacuum grease used during synthesis; however, no fluorine was detected by elemental combustion analysis. This indicates that the contamination was present only on the surface. The highest C/O ratios were obtained for HU/H/Zn (16.2) and for HU/D/Zn (14.2). Comparing these results with Raman spectroscopy data, we can conclude that high D/G ratio originated mostly from defects induced by reduction. A relatively high C/O ratio was determined for ST/H/Zn (12.2). The lowest values of C/O ratios were obtained for HO/H/Zn (8.6), HO/D/Zn (9.9) and BR/H/Zn (8.8). The results of XPS analysis are summarized in **Table 4**. Let us note, that such a high C/O ratio is comparable with the thermally reduced graphene and is significantly higher than typical values observed on chemically reduced graphene.[30]

Table 4. The composition of graphite oxides exposed to Clemmensen reduction under different conditions (HCl/DCl) by XPS in at.%.

Sample	C	O	C/O
HO/H/Zn	89.6	10.4	8.6
HO/D/Zn	90.8	9.2	9.9
HU/H/Zn	94.2	5.8	16.2
HU/D/Zn	93.4	6.6	14.2
BR/H/Zn	92.4	7.6	12.2
ST/H/Zn	89.8	10.2	8.8

The deconvolution of C 1*s* peak was performed to obtain information about bonding conditions and relative concentration of individual functionalities (**Fig. 6**). Six different carbon bonds were assumed: the C=C (284.5 eV), the C-C/C-H (285.5 eV), the C–O of alcohol/ether groups (286.3 eV), the C=O of carbonyl groups (288 eV), O–C=O of carboxylic acid/ester groups (289 eV) and the π–π^* interactions (291 eV). The results of deconvolution for C 1*s* are shown in **Table 5**. Only small differences were identified between the respective samples which indicates a similar reduction mechanism with hydrogen and deuterium without any significant isotopic kinetic effect. The peak at 285.5 eV is attributed to both the C-H and C=C bond due to their similar energies, therefore this XPS cannot give an exact evidence of C-H bond. The high degree of reduction was also documented by high resolution O 1*s* spectra where only single peak at 532.5 eV correlated with C-O bond is dominantly present after reduction (**Fig. S2**).

Table 5. The different bonding arrangements in graphite oxides exposed to Clemmensen reduction under different conditions (HCl/DCl) based on HR-XPS analysis by deconvolution of C 1*s* peak (in %).

Sample	C=C	C-C/ C-H	C-O	C=O	O-C=O	π - π^*
HO/H/Zn	62.7	14	2.3	9.4	0.6	11
HO/D/Zn	54.1	18.6	8.8	8.8	2.1	7.6
HU/H/Zn	55.6	13.7	8.6	6.1	7.7	8.3
HU/D/Zn	55	16.8	2.5	7.4	4.5	13.8
ST/H/Zn	54.5	16.2	6	8.5	6.6	8.2
BR/H/Zn	52.4	19.5	6.2	9.1	4.8	8

In order to resolve the mechanism of the Clemmensen reduction we applied various geometrical arrangements of the substrate (graphite oxide) and the reducing agent (zinc). This could not be applied for simple small molecules in a solution, but the large graphene sheets can be arranged in various experimental configurations and subsequently analyzed by different characterization techniques. We performed two different experiments. For the first experiment we placed HO-GO in direct **contact with metal** (sample was termed HO-C) while for the second one HO-GO was kept away from the metal, where only active (**nascent**) hydrogen formed by dissolution of zinc came into contact with HO-GO (sample was termed HO-N). These samples were analyzed by various methods after four hours in reaction environment.

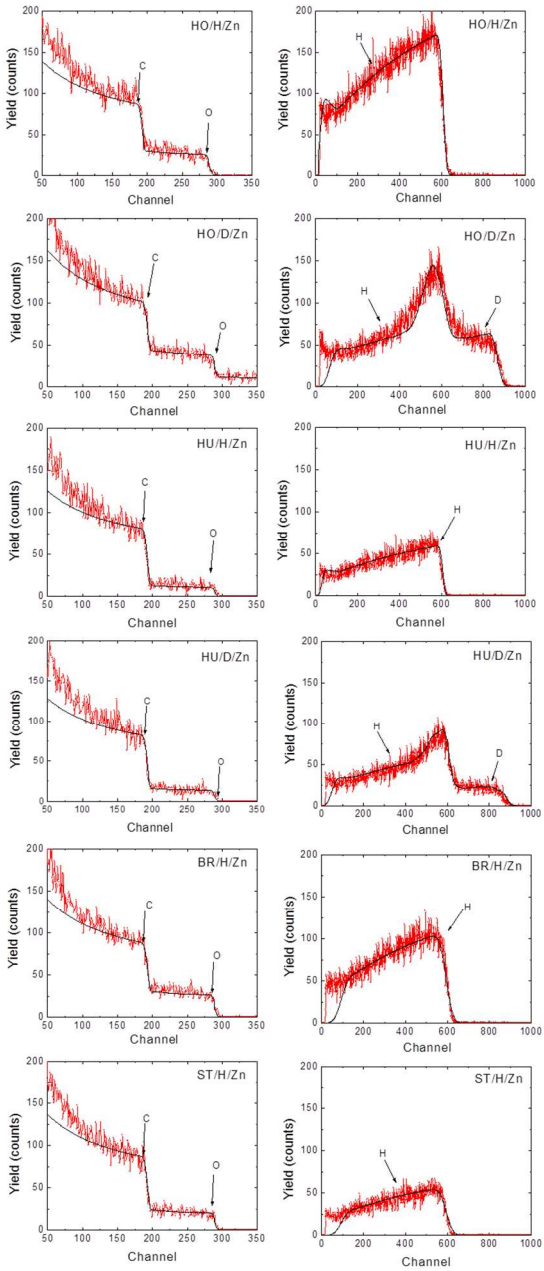

Fig. 4 Rutherford back scattering (left) and elastic recoil detection analysis (right). Red lines represent the experimental data while the simulated profiles are depicted in black.

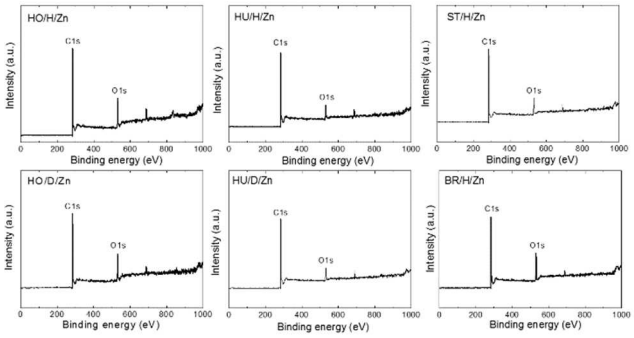

Fig. 5 XPS survey spectra of graphite oxides exposed to Clemmensen reduction under different conditions (HCl/DCl).

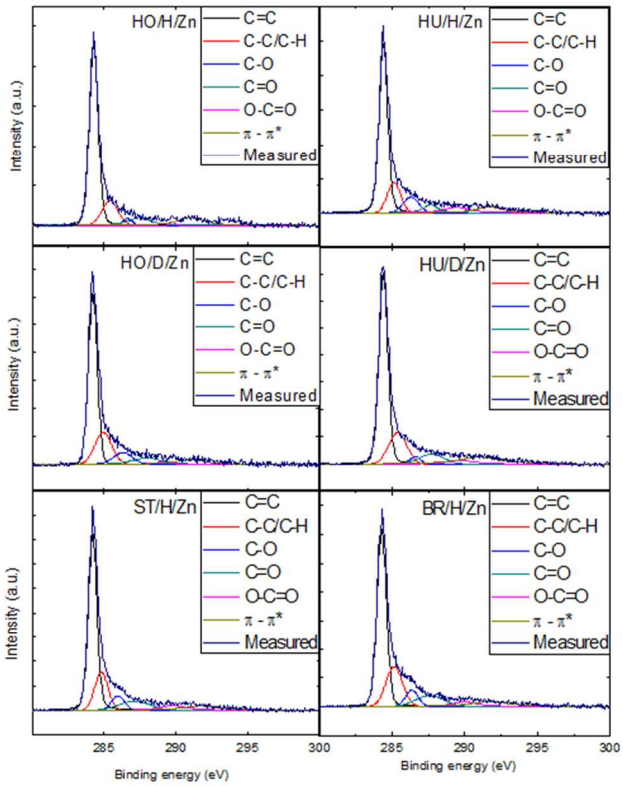

Fig. 6 The deconvolution of C 1*s* peak of graphite oxides exposed to Clemmensen reduction under different conditions (HCl/DCl).

To examine the reduction of C=O functional group FT-IR measurement was performed for HO-C and HO-N and also for HO-GO (for the comparison) (**Fig. 7**). The significant reduction of C=O vibration band intensity (1630 cm^{-1}) is clearly visible for HO-C sample. The vibration band originated from C-O vibration in OH groups remained almost unchanged (1290 cm^{-1}, 1190 cm^{-1} and 1130 cm^{-1}). The vibration band originated from C-O band of epoxide ring are suppressed for both samples (1000 cm^{-1} and 870 cm^{-1}) and indicate high reactivity of these functional groups in graphite oxide. The vibration band at ~1520 cm^{-1} originated from graphene skeleton. In contrast, HO-N still exhibits the band at energy 1630 cm^{-1} confirming that the direct contact of C=O group with Zn is required for the Clemmensen reduction to proceed.

The XPS analysis results showed significant differences between HO-C and HO-N (**Fig. 8**). On the O 1*s* peak we observed a nearly complete disappearance of C=O bond for HO-C sample. The same effect was identified for C 1*s*, where also a significant decrease of C=O concentration was found compared to HO-N (see **Table 6**). This resulted in much higher C/O ratio for HO-C (4.8 for HO-C and 2.7 for HO-N). The C/O ratio in HO-N is almost identical with that of HO-GO (2.8) indicating almost negligible extent of reduction. A relatively high concentration of carboxylic acid functional groups on HO-C suggests that these functional groups are not affected by Zn/HCl reduction which is in agreement with reactions performed on small organic molecules.

These exceptionally interesting findings allowed us to conclude that the mechanism of Clemmensen reduction should be based on the carbenoid mechanism. The following reaction scheme (**Scheme 2**) based on our observations illustrates the reduction of HO-GO in direct contact with zinc (sample HO-C).

Table 6. The C 1*s* peak deconvolution for samples HO-C (contact with Zn) and HO-N (no contact with Zn).

Sample	C=C	C-C C-H	C-O	C=O	O-C=O	π-π*
HO-C	34.8	43.3	8.1	2.3	9.3	2.2
HO-N	23.2	11.2	26.5	10.5	25.4	3.1

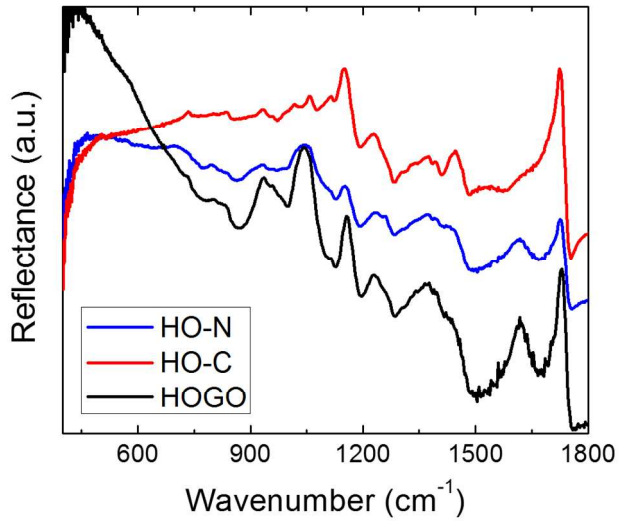

Fig. 7 FT-IR spectra of starting graphite oxide (HOGO) and HOGO reduced in contact (HO-C) and without contact with zinc metal (HO-N).

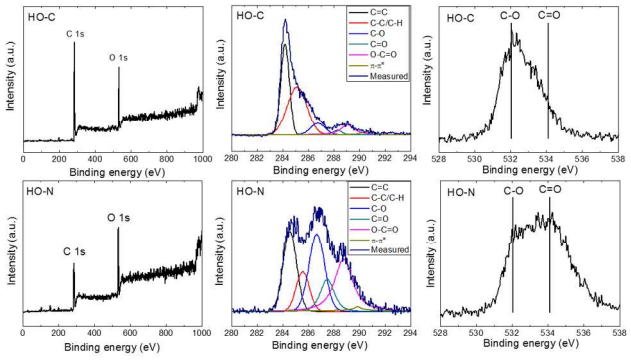

Fig. 8 XPS survey spectra (left), fitted high resolution C 1*s* peak (middle) and O 1*s* peak (right) of GO reduced in contact with Zn (C) and without the direct contact with Zn metal (N).

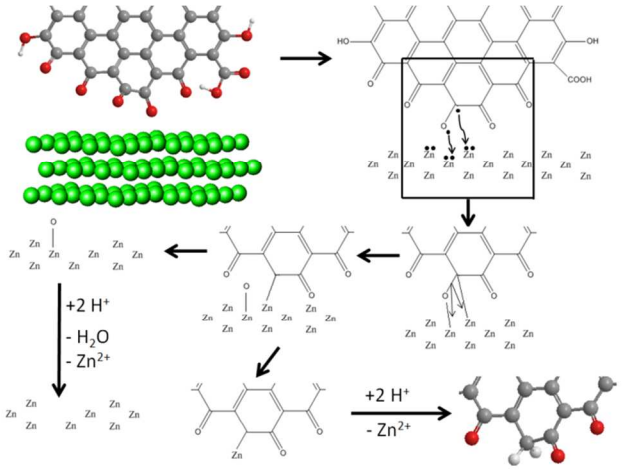

Scheme 2. The mechanism of ketone group reduction on graphite oxide. The Zn atoms in the scheme mean zinc metal surface.

Conclusions

The reduction / hydrogenation of various graphite oxides by zinc in hydrochloric acid was investigated in details. Deuterium labeling was applied to assess the exact degree of graphite hydrogenation. The amount of deuterium was estimated using nuclear methods of material analysis – RBS and ERDA. Additionally the topological approach was applied in order to identify the mechanism of graphite oxide reduction by zinc in acidic environment – Clemmensen reduction. The results indicate that the reduction / hydrogenation of the ketonic groups proceeds only in contact with the surface of zinc metal whereas the so called "nascent hydrogen" affects only the reduction of highly reactive oxygen functional groups such as epoxides. The combination of such analytic techniques allowed us to understand the role of Zn in the mechanism of Clemmensen reduction and to exactly determine the degree of hydrogenation. In addition, this study is essential for future investigation of various reaction mechanisms, where similar approach can be applied. Graphite oxide with higher concentration of ketone functional groups can be further applied for synthesis of highly hydrogenated graphene or even pure graphane.

Acknowledgements

The project was supported by Czech science foundation (project GACR No. 15-09001S) and by Specific University Research (MSMT no. 20/2015). RBS and ERDA analysis was realized at CANAM (Center of Accelerators and Nuclear Analytical Methods) LM 2011019.

Notes and references

[a], Department of Inorganic Chemistry, University of Chemistry and Technology, 166 28 Prague 6, Czech Republic. E-mail: zdenek.sofer@vscht.cz; Fax: +420 22431-0422
[b] Nuclear Physics Institute of the ASCR, v. v. i., 250 68 Řež, Czech Republic. E-mail: mackova@ujf.cas.cz
[c] Department of Physics, Faculty of Science, J.E. Purkine University, 400 96 Ustí nad Labem, Czech Republic
[d] Division of Chemistry & Biological Chemistry, School of Physical and Mathematical Sciences, Nanyang Technological University, Singapore, 637371, Singapore. E-mail:pumera@ntu.edu.sg; Fax: +65 6791-1961

† Footnotes should appear here. These might include comments relevant to but not central to the matter under discussion, limited experimental and spectral data, and crystallographic data.
Electronic Supplementary Information (ESI) available: [details of any supplementary information available should be included here]. See DOI: 10.1039/b000000x/

1. A. K. Geim and K. S. Novoselov, *Nat. Mater.*, 2007, **6**, 183-191.
2. Z. Sofer, O. Jankovský, P. Šimek, K. Klímová, A. Macková and M. Pumera, *ACS Nano*, 2014, **8**, 7106-7114.
3. O. Jankovsky, P. Simek, D. Sedmidubsky, S. Matejkova, Z. Janousek, F. Sembera, M. Pumera and Z. Sofer, *RSC Advances*, 2014, **4**, 1378-1387.
4. O. Jankovsky, P. Simek, K. Klimova, D. Sedmidubsky, S. Matejkova, M. Pumera and Z. Sofer, *Nanoscale*, 2014, **6**, 6065-6074.
5. D. Elias, R. Nair, T. Mohiuddin, S. Morozov, P. Blake, M. Halsall, A. Ferrari, D. Boukhvalov, M. Katsnelson and A. Geim, *Science*, 2009, **323**, 610-613.
6. J. O. Sofo, A. S. Chaudhari and G. D. Barber, *Physical Review B*, 2007, **75**, 153401.
7. Z. Sofer, O. Jankovsky, P. Simek, L. Soferova, D. Sedmidubsky and M. Pumera, *Nanoscale*, 2014, **6**, 2153-2160.
8. T. Hussain, B. Pathak, T. A. Maark, C. M. Araujo, R. H. Scheicher and R. Ahuja, *EPL (Europhysics Letters)*, 2011, **96**, 27013.
9. M. Pumera and C. H. A. Wong, *Chem. Soc. Rev.*, 2013, **42**, 5987-5995.
10. F. Bonaccorso, Z. Sun, T. Hasan and A. C. Ferrari, *Nat. Photonics*, 2010, **4**, 611-622.
11. L. Xie, L. Jiao and H. Dai, *J. Am. Chem. Soc.*, 2010, **132**, 14751-14753.
12. J. S. Burgess, B. R. Matis, J. T. Robinson, F. A. Bulat, F. K. Perkins, B. H. Houston and J. W. Baldwin, *Carbon*, 2011, **49**, 4420-4426.
13. H. L. Poh, F. Šaněk, Z. Sofer and M. Pumera, *Nanoscale*, 2012, **4**, 7006-7011.
14. S. Pekker, J.-P. Salvetat, E. Jakab, J.-M. Bonard and L. Forro, *The Journal of Physical Chemistry B*, 2001, **105**, 7938-7943.
15. P. Kumar, K. Subrahmanyam and C. Rao, *Materials Express*, 2011, **1**, 252-256.
16. E. Clemmensen, *Berichte der deutschen chemischen Gesellschaft*, 1913, **46**, 1837-1843.
17. M. L. Di Vona and V. Rosnati, *The Journal of Organic Chemistry*, 1991, **56**, 4269-4273.
18. J. H. Brewster, *J. Am. Chem. Soc.*, 1954, **76**, 6364-6368.
19. V. H. Pham, H. D. Pham, T. T. Dang, S. H. Hur, E. J. Kim, B. S. Kong, S. Kim and J. S. Chung, *J. Mater. Chem.*, 2012, **22**, 10530-10536.
20. W. Hummers and R. Offeman, *J. Am. Chem. Soc.*, 1958, **80**, 1339–1339.
21. U. Hofmann and A. Frenzel, *Kolloid-Z.*, 1934, **68**, 149–151.
22. B. C. Brodie, *Ann. Chim. Phys.*, 1860, **1860**, 466–472.
23. L. Staudenmaier, *Berichte Dtsch. Chem. Ges.* , 1898, **31**, 1481–1487.
24. C. K. Chua and M. Pumera, *Chem. Soc. Rev.*, 2014, **43**, 291-312.
25. C. K. Chua, Z. Sofer and M. Pumera, *Chemistry – A European Journal*, 2012, **18**, 13453-13459.
26. M. Mayer, *Nuclear Instruments and Methods in Physics Research Section B: Beam Interactions with Materials and Atoms*, 2014, **332**, 176-180.
27. J. Saarilahti and E. Rauhala, *Nuclear Instruments and Methods in Physics Research Section B: Beam Interactions with Materials and Atoms*, 1992, **64**, 734-738.
28. A. C. Ferrari, J. C. Meyer, V. Scardaci, C. Casiraghi, M. Lazzeri, F. Mauri, S. Piscanec, D. Jiang, K. S. Novoselov, S. Roth and A. K. Geim, *Phys. Rev. Lett.*, 2006, **97**, 187401.
29. L. G. Cancado, K. Takai, T. Enoki, M. Endo, Y. A. Kim, H. Mizusaki, A. Jorio, L. N. Coelho, R. Magalhaes-Paniago and M. A. Pimenta, *Appl. Phys. Lett.*, 2006, **88**, 163106-163106-163103.

30. P. Šimek, Z. Sofer, O. Jankovský, D. Sedmidubský and M. Pumera, *Adv. Funct. Mater.*, 2014, **24**, 4878-4885.